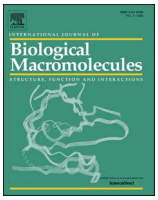
International Journal of Biological Macromolecules 306 (2025) 141806



Contents lists available at ScienceDirect

International Journal of Biological Macromolecules

journal homepage: www.elsevier.com/locate/ijbiomac





Mirror substrates specificity of a 2, 3-dihydroxypropanesulfonate degrading enzyme in sulfate-reducing bacteria

Xiaoyi Ma [1], Huanyu Wang [1], Le Liu, Hongyue Dang, Kai Tang [*]

State Key Laboratory of Marine Environmental Science, Fujian Key Laboratory of Marine Carbon Sequestration, College of Ocean and Earth Science, Xiamen University, Xiamen, China

ARTICLE INFO

Keywords:
Chirality
Enzyme
Organosulfur
Anaerobic bacteria

ABSTRACT

Ubiquitous *R*- and *S*-enantiomers of 2,3-dihydroxypropanesulfonate (DHPS), organic sulfur compounds produced by photosynthetic organisms, serve as common nutrient and energy sources for specific bacteria. While most known DHPS-degrading enzymes exhibit enantioselectivity, this study introduces a unique dehydrogenase, DhpA from the sulfate-reducing bacterium *Desulfovibrio* sp. DF1, capable of efficiently metabolizing both *R*- and *S*-DHPS to 3-sulfolactaldehyde (SLA). The crystal structure of DhpA reveals a conserved binding pocket that recognizes the sulfonate group of DHPS through interactions with Lys123, Ser174, and Asn175. The catalytic mechanism of the enzyme involves the oxidation of the C3-OH group of both enantiomers, facilitated by the Lys171. The mutation of Lys171 significantly diminishes activity, confirming its critical role in catalysis. Based on biochemical and genetic analyses, this study proposes a chiral DHPS degradation pathway in bacteria. This study reveals the unique enantiomeric selectivity of DhpA, expanding our understanding of the bacterial metabolism of chiral molecules.

1. Introduction

Natural products, characterized by structural complexity, diversity and chirality, exist in well-defined stereo-configurations, reflecting the chiral nature of the natural environment [1,2]. Amino acids, among the most extensively studied chiral molecules, are typically classified as *L*- and *D*-enantiomers [3,4]. While *L*-amino acids primarily serve as protein building blocks and precursors for various sulfonates (e.g., isethionate, DHPS, and sulfolactate) [5,6], while *D*-amino acids are found in bacterial cell wall peptidoglycans and act as ligands for neurotransmitter molecules involved in signal transduction [7,8]. The presence of these enantiomers necessitates enzymes with stereoselectivity in substrate recognition [9]. For example, *L*- and *D*-amino acid oxidases exhibit strict chiral selectivity towards their respective substrates [9]. Similarly, *R*- and *S*-hydroxypropylthioethanesulfonate dehydrogenase demonstrate oxidation activity only with its corresponding substrate [10]. This chiral selectivity ensures the accuracy and efficiency of biochemical reactions within cells, potentially converting harmful compounds into metabolizable substances [11,12]. However, some microbial enzymes exhibit weaker stereoselectivity towards enantiomeric substrates, and these enzymes are typically identified as lipases. For example, the wild-type bacterial lipase from *Pseudomonas aeruginosa* can act on both *R*- and *S*-2 methyldecanoic acid *p*-nitrophenyl ester [13,14]. The lipase from *Pseudomonas cepacia* shows a preference for the *R*-trioctyl compound over the *S*-trioctyl compound [15]. These examples suggest that the catalytic selectivity of enzymes for chiral enantiomeric substrates is not always absolute.

Chiral DHPS is a prominent organic sulfur compounds widely distributed in both terrestrial and marine environments [16,17]. A significant pathway for DHPS production involves the catabolism of sulfoquinovose (SQ), a crucial component of sulfolipids found in photosynthetic organism, with an estimated annual global production of 10 billion tons, through the sulfoglycolytic Embden-Meyerhof-Parnas pathway [18,19]. Marine algae, such as diatoms and dinoflagellates, are key producers of DHPS. These organisms can synthesize at least one enantiomer of DHPS, achieving intracellular concentrations ranging from 5 to 18 mM [17]. A diverse range of bacteria possess the metabolic capacity to degrade DHPS, utilizing it as a source of carbon, sulfur, and energy. This includes aerobic like *Roseobacteraceae* bacteria [20], *Klebsiella* sp. ABR11, *Cupriavidus pinatubonensis* [21], as well as anaerobic sulfate-reducing bacteria *Desulfovibrio* sp. DF1 [22], *Bilophila wadsworthia* and *Klebsiella oxytoca* [23]. The metabolic pathways employed

* Corresponding author.
E-mail address: tangkai@xmu.edu.cn (K. Tang).
[1] Authors contributed equally: Xiaoyi Ma, Huanyu Wang.

https://doi.org/10.1016/j.ijbiomac.2025.141806
Received 22 October 2024; Received in revised form 27 December 2024; Accepted 4 March 2025
Available online 5 March 2025
0141-8130/© 2025 Elsevier B.V. All rights are reserved, including those for text and data mining, AI training, and similar technologies.

by these bacteria play a crucial role in the mineralization of organic sulfur, driving its cycling within the environment. Enantioselectivity is a notable characteristic of DHPS degradation. *Roseobacter* bacteria can metabolize both *R*- and *S*-DHPS [20]. Furthermore, enzymes such as HpsO, HpsP, and HpsN in *Roseobacteraceae* strains exhibit remarkable substrate specificity, differentiating between the primary hydroxyls of *R*- and *S*-DHPS isomers and catalyzing their oxidation to produce sulfolactaldehyde [24]. Similarly, *Cp*HpsN from *C. pinatubonensis* demonstrates strict stereospecificity, exclusively catalyzing oxidation of *R*-DHPS [25]. Anaerobic bacteria utilize distinct degradation pathway, often involving the cleavage of C—S and C—O bonds within the DHPS molecule [23]. While sulfate-reducing bacteria like *Desulfovibrio* sp. DF1, isolated from sewage sludge are known to convert DHPS sulfur to hydrogen sulfide (H_2S) [22], the biochemical pathway for DHPS degradation is still not fully understood. Furthermore, our understanding of the molecular mechanisms underlying catalysis by DHPS dehydrogenase (DhpA) is currently limited.

Here, we present kinetic and structural analyses of DHPS-dehydrogenase DhpA from *Desulfovibrio* sp. DF1, revealing its stereospecificity and unique ability concurrently to catalyze two enantiomeric substrates. Furthermore, we determined the crystal structure of DhpA using X-ray crystallography and analyzed its catalytic mechanism for *R*- and *S*-DHPS, as well as proposing the DHPS degradation pathway. Our findings illuminate the intricate interplay between DhpA and chiral substrates, demonstrating the enzyme's remarkable specificity and versatility. These insights provide valuable information for understanding enzyme-substrate interactions and optimizing enzyme catalytic reactions.

2. Materials and methods

2.1. Expression and purification of DhpA

The *dhpA* gene (gene locus tag: Ga0134130_130620) from *Desulfovibrio* sp. DF1 was synthesized by Sangon Biotech (Shanghai, China) and cloned into the pCold II vector using *Nde*I/Xhol restriction sites. Site-directed mutagenesis was performed using the Mut Express II Fast mutagenesis kit V2 (Vazyme, Nanjing, China) to introduce desired mutations (mutagenic primers listed in Supplementary Table S1).

Recombinant plasmids were then transformed into *Escherichia coli* BL21 (DE3) cells. Briefly, *E. coli* BL21 cells were cultured in LB liquid medium at 37 °C until the optical density at 600 nm (OD_{600}) reached 0.6–0.8. The culture was then expanded for further growth until an OD_{600} reached approximately 0.6. Isopropyl *β*-D-thiogalactoside was added to a final concentration of 0.5 mM to induce protein expression, followed by incubation at 16 °C for 24 h. Cells were harvested by centrifugation, resuspended in a buffer (10 mM Tris-HCl, pH 8.0, 150 mM NaCl), and lysed by sonication. The cell lysate was clarified by centrifugation and filtered through a 0.22 μm membrane (Merck Millipore).

Protein purification was carried out using an AKTA pure system (Cytiva, MA, USA). The cell lysate was loaded onto a 5 mL HisTrap HP column (Cytiva, MA, USA). The sample was loaded onto the column at a flow rate of 1 mL/min and eluted with imidazole-containing buffers at various concentrations (4 %, 10 %, and 50 %). The purified protein was analyzed by SDS-PAGE on a commercial gel (precast protein plus gel, Hepes-Tris, 4–20 %). High-purity samples were further purified using a desalting column (5 mL, Cytiva) with phosphate buffer (10 mM, pH 8.0), concentrated, and stored at −80 °C for further use.

2.2. Enzymatic assay for DhpA

A 200 μL reaction mixture containing 10 mM phosphate buffer (PB), pH 8.0, 10 μM DhpA, 10 mM NAD^+, and 10 mM *R*- or *S*-DHPS was added to each well of a 96-well plate. The time-dependent increase in NADH absorbance mediated by DhpA was monitored photometrically at 340 nm using a plate reader for 5 min (Tecan M200, Männedorf, Switzerland). Negative controls lacking DhpA were included in each experiment. All experiments were performed in triplicate. To determine Michaelis-Menten kinetic parameters, a 200 μL reaction mixture containing 10 mM PB buffer, 10 mM NAD^+, and varying concentrations of *R*- or *S*-DHPS was prepared in each well of a 96-well plate while maintaining a constant DhpA concentration. The change in absorbance at 340 nm was monitored to determine the reaction rate.

2.3. Determination of the affinities of R- and S-DHPS to DhpA by surface plasmon resonance (SPR) measurements

DhpA (concentration > 1 mg/mL) containing the DHPS binding site, was analyzed using SPR. A two-channel coupling was performed on a Series S Sensor Chip CM5 (Cytiva). Channel 1 served as a reference (closed coupling), while channel 2 was used for immobilizing DhpA. A 70 % glycerol solution was used for normalization. To optimize binding conditions, DhpA were sequentially flowed through both channels using four sodium acetate-acetic acid buffers with varying pH (4.0, 4.5, 5.0, 5.5). pH 4.0 was determined to be optimal for protein binding and was subsequently used for immobilization on the sensor chip surface. A series of concentrations of *R*- or *S*-DHPS small molecule substrates were then injected into the flow system at 25 °C. The equilibrium dissociation constants (K_D) of *R*- and *S*-DHPS were determined by analyzing the resulting sensorgrams using Biacore T200 Evaluation Software.

2.4. Protein crystallization and data collection, processing, and refinement

The protein was further purified using a gel filtration column (Superdex 200 Increase 10/300 GL, Cytiva), resulting in a purity of >95 % and a concentration of 20 mg/mL. DhpA crystals were grown at 18 °C using the sitting-drop vapor diffusion method with a reservoir solution containing 0.2 M $MgCl_2$, 25 % *w/v* polyethylene glycol 3350, and 0.1 M HEPES (pH 7.5). Crystals were harvested with nylon CryoLoops (Hampton Research) and soaked in the reservoir solution containing 20 % glycerol as a cryoprotectant. Diffraction data were collected at 100 K from a single crystal at the Shanghai Synchrotron Radiation Facility BL18U beamline (China) using a wavelength of 0.97 Å. The diffraction data were processed and scaled with XDS [26]. The structure of DhpA was solved at 2.88 Å resolution by molecular replacement using the protein structure (PDB ID: 3CKY) as a template [27]. Structure building and refinement were performed using Coot [28] and Phenix [29]. The stereochemical quality of the final model was assessed with Procheck [30]. Detailed data collection and refinement statistics are provided in Supplementary Table S2.

2.5. Molecular docking and dynamics simulation

For molecular docking, DhpA was superimposed onto the 3-sulfolactaldehyde reductase (PDB ID: 6SMY) and 3-dehydro-2-deoxy-D-gluconate dehydrogenase complexed with NAD^+ (PDB ID: 2CVZ) [31,32], resulting in a root-mean-square deviation (RMSD) deviation of 1.87 Å and 2.4 Å, respectively. After removing the other two protein structures, DhpA was docked with *R*- and *S*-DHPS, respectively. Protein superposition was performed using the US-align online tool [33]. AutoDock 4 was used for docking, with Gasteiger charges and hydrogen atoms were added to both proteins and ligands [34]. The genetic algorithm was employed with a medium setting for the maximum number of evaluations. Conformations with the lowest binding energies were selected for subsequent molecular dynamics simulations.

Molecular dynamics simulations were conducted using the NAMD program package [35] based on the docking as the initial structures for DhpA·DHPS·NAD^+. The DhpA-ligand complex model was placed in an orthorhombic box containing water molecules, sodium and chloride ions to neutralize the system. Sodium and chloride ions were randomly

dispersed within the solvation systems under periodic boundary conditions. The system was minimized for 1 ns to reach equilibrium, followed simulation at 300 K. The resulting structures were visualized and analyzed with Pymol (http://www.pymol.org/).

2.6. Bioinformatic analysis

Phylogenetic analysis of sulfate-reducing bacteria was performed using IQ-TREE (http://iqtree.cibiv.univie.ac.at) [36]. Single-copy genes identified for this analysis are detailed in the Supplementary Table S3. These genes were aligned using ClustalW [37]. A maximum likelihood approach (model: LG + F + G4) based on the aligned amino acid sequences was employed for tree construction. Bootstrap support values were calculated and visualized with FigTree v1.4.4. The protein structures of *Om*DhpA (WP_144306080.1) from *Oceanidesulfovibrio marinus* P48SEP, *Dr*DhpA (Dret_2323) from *Desulfohalobium retbaense* DSM 5692, *Dt*DhpA (LZ09DRAFT_00491) from *Desulfonatronum thioautotrophicum* ASO4–1, *Dla*DhpA (DeslaDRAFT_3103) from *Desulfonatronum lacustre* DSM 10312, *Dl*DhpA (EJ49DRAFT_01517) from *Desulfovibrio litoralis* DSM 11393, and *Da*DhpA (Ga0615370_01_7208805_7209665) from *Desulfosarcina alkanivorans* PL12 were predicted using AlphaFold 2 [38]. The amino acid sequences of these proteins were compared using MAFFT [39], and the results were visualized using ESPript 3 [40].

3. Results

3.1. Identification and biochemical characterization of DhpA

We recombinantly produced DhpA from *Desulfovibrio* sp. DF1, exhibiting an approximate molecular weight of 30 kDa (Fig. 1A). Biochemical characterization revealed that DhpA utilizes both *R*- and *S*-DHPS as substrates, demonstrating NAD^+- dependent catalytic activity (Fig. 1B). Kinetic analyses revealed the following parameters for *R*-DHPS: $k_{cat} = 16.87 \pm 2.40\ s^{-1}$, $K_M = 1.27 \pm 0.26$ mM, $k_{cat}/K_M = 13.28 \pm 1.88\ mM^{-1}\ s^{-1}$. DhpA displayed higher catalytic activity with *S*-DHPS as a substrate ($k_{cat} = 19.28 \pm 1.20\ s^{-1}$, $K_M = 1.14 \pm 0.13$ mM, $k_{cat}/K_M = 16.91 \pm 1.05\ mM^{-1}\ s^{-1}$) (Fig. 1C and D), exhibiting a 1.14-fold preference for *S*-DHPS in terms of k_{cat}/K_M. SPR experiments demonstrated comparable binding affinities of both *R*- and *S*-DHPS to DhpA, with K_D of 0.91 mM and 0.88 mM, respectively (Fig. 1E and F). Collectively, these findings confirm the non-stereospecificity nature of DhpA with respect to DHPS affinity and catalytic rates.

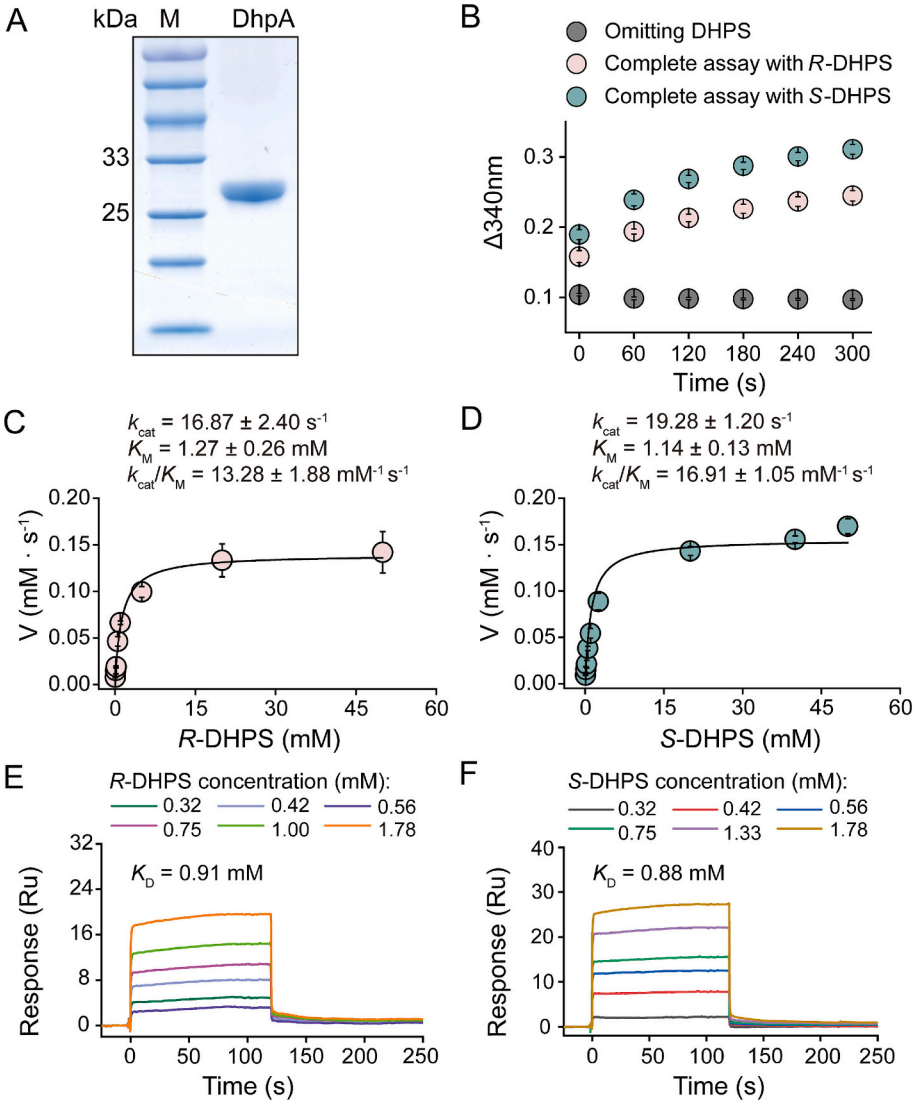


Fig. 1. Enzymatic assay of DhpA. (A) SDS-PAGE analysis of purified DhpA. Lane M, protein molecular weight marker; lane DhpA, purified DhpA. (B) DhpA enzyme activity assay with *R*- and *S*-DHPS as substrates, respectively. (C) Michaelis-Menten plot for the oxidation of *R*- and *S*-DHPS (D) by DhpA from *Desulfovibrio* sp. DF1, respectively. (E) SPR measurement of the binding of *R*- and *S*-DHPS (F) to DhpA, respectively. Error bars correspond to the standard deviation ($n = 3$).

3.2. Crystal structure of DhpA

To elucidate the molecular basis of DhpA catalysis, the crystal structure of DhpA was determined using molecular replacement. A bacterial β-hydroxyacid dehydrogenase (Hgd, PDB ID: 3CKY) with 32 % sequence similarity served as the search model [27]. The DhpA structure exhibited high structural similarity to Hgd, with an RMSD of 1.37 Å. DhpA crystallized in space group I4122, and the 3D structure was subsequently solved and refined to a resolution of 2.88 Å (Supplementary Table S2). Structural analysis revealed that the DhpA crystal contains three monomeric units in the asymmetric unit (Fig. 2A). Each monomer comprises eight β-strands and thirteen α-helices (Fig. 2B), exhibiting high structural similarity with RMSD values of 0.19–0.32 Å between the three monomers. Each DhpA monomer consists of two distinct domains: an N-terminal Rossmann-fold domain (residues 1–164) for dinucleotide binding and a C-terminal domain (residues 165–286) composed of six helices (Fig. 2B and C). Docking simulations of DhpA, NAD^+ and either *R*- or *S*-DHPS, followed by molecular dynamics refinement, revealed that the ligands occupy the cleft between the N- and C-terminal domains. The N-terminal domain harbors a conserved NAD^+ cofactor recognition motif (GXXGXGXMGXXXAXNXXXXG, residues 4–23, where X represents any residue), characteristic of NAD/NADP-dependent dehydrogenases [32]. In the DhpA·NAD^+·DHPS complexes, the DHPS molecule is positioned near the nicotinamide ring of NAD^+. The C3 of *R*- and *S*-DHPS are positioned within suitable distance (~5.0 Å and ~ 4.9 Å, respectively) from the C4 atom of the nicotinamide ring for hydride transfer and subsequent DHPS oxidation. Furthermore, hydrogen bond interactions between the C2-OH and C3-OH of the nicotinamide ribose of the cofactor and the residues Thr96 and Asp240 (Fig. 2E and F) suggest their direct involvement in cofactor coordination.

A structure-based search using Foldseek with DhpA structure as a query identified *Escherichia coli* K-12 3-sulfolactaldehyde reductase (YihU, PDB: 6SMY) as structural homolog [31,41]. Despite a low sequence identity (~30 %), the DhpA structure exhibits significant

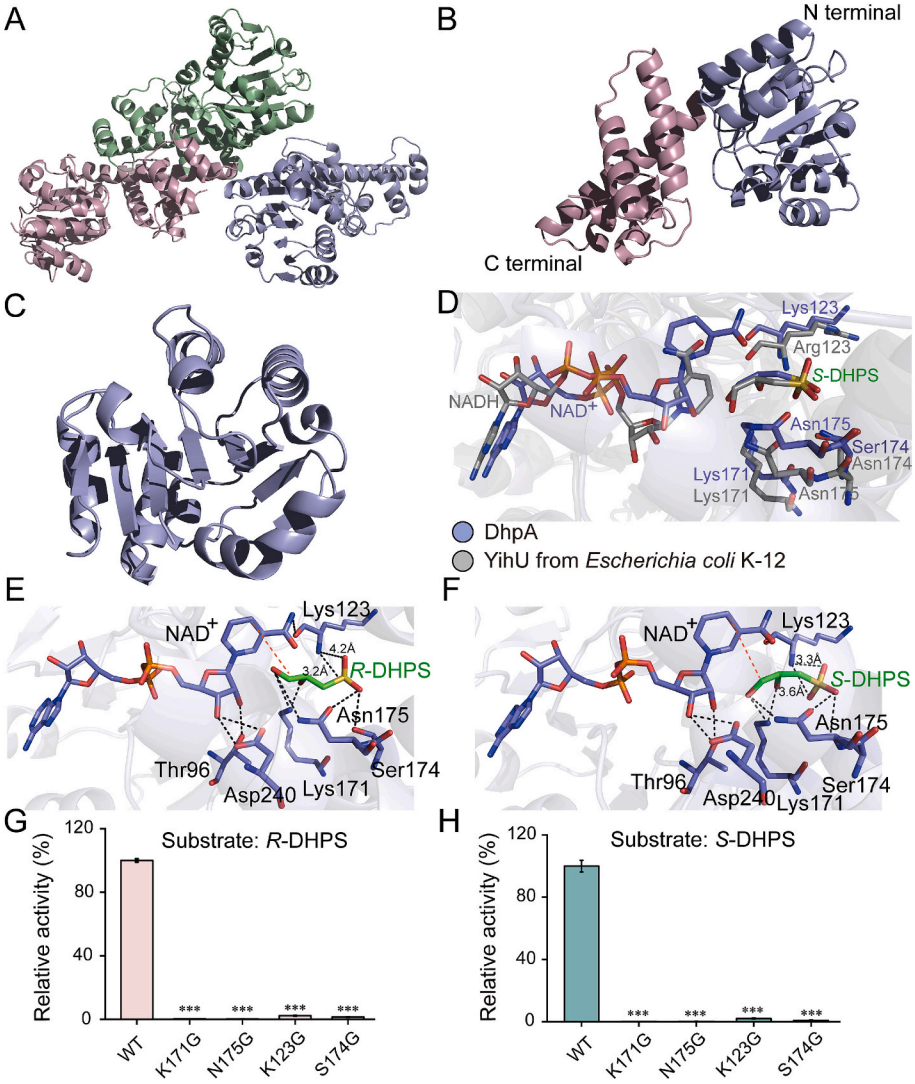


Fig. 2. Structure and functional analysis of DhpA. (A) Overall structure of the DhpA in the asymmetric unit. (B) The DhpA monomer can be divided into a N-terminal domain (purple) and a C-terminal domain (pink). (C) Cartoon diagram of the DhpA monomer, revealing a typical Rossmann-like fold comprising eight parallel β-strands sandwiched between seven α-helices. (D) Superposition of the structures of DhpA·NAD^+·*S*-DHPS (purple) and YihU·NADH·*S*-DHPS (grey, PDB ID: 6SMY), highlighting differences in catalytic and sulfonate-binding residues. (E) Structure details of DhpA in complex with NAD^+ and *R*-DHPS or *S*-DHPS (F). The catalytic residues Lys171 and active site residues Ser174, Asn175, and Lys123 are shown as sticks. Black dashed lines indicate hydrogen bonds. Black dashed lines indicate hydrogen bonds. Orange dashed line illustrates the hydride transfer path between C4 of the nicotinamide ring and the C3-atom of the *R*- or *S*-DHPS. (G) Relative enzymatic activities of wild-type DhpA, mutant variants (K123A, K171G, S174G and N175G) towards *R*-DHPS and *S*-DHPS (H), respectively. The activity of wild type DhpA was set as the reference (100 %). ***, $p < 0.001$ (*t*-test). Error bars correspond to the standard deviation (n = 3).

structural similarity to YihU, with an RMSD of 1.87 Å (Fig. 2D). In YihU, Lys171 is proposed to function as a general acid catalyst, while a triad of residues (Arg123, Asn174, and Ser178) is involved in sulfonate binding [31]. Superposition of the DhpA·NAD^+·*S*-DHPS and YihU·NADH·*S*-DHPS complexes demonstrates the structural conservation of Lys171 (Lys171 in DhpA) (Fig. 2D). The backbone amide N—H of Lys171 in DhpA forms hydrogen bonds with the C2-OH and C3-OH of *R*- or *S*-DHPS, respectively (Fig. 2E and F). Simultaneously, the C3-OH and a sulfonate oxygen of DHPS form hydrogen bonds with the backbone amide group of Asn175, which is conserved in YihU (Asn175) (Fig. 2D). The Lys171 and Asn175 residues in DphA are conserved in β-hydroxyacid dehydrogenases, where they serve as catalytic residues [27,42,43], suggesting that Lys171 and Asn175 in DhpA may have similar function. Lys171 likely acts as a catalytic base, abstracting a proton from the hydroxyl group of *R*- or *S*-DHPS. Concurrently, Asn175 stabilizes the negatively charged intermediate of DHPS formed upon deprotonation by Lys171. Consistent with these proposed roles, mutating Lys171 or Asn175 to Gly abolished DhpA activity towards both *R*- and *S*-DHPS (Fig. 2G and H), highlighting the critical importance of these residues for catalysis. While maintaining a similar binding mode for both *R*- and *S*-DHPS (Fig. 2E and F), DhpA exhibits distinct active site interactions compared to YihU. In YihU, Arg123 and Asn174 occupy positions equivalent to Lys123 and Ser174 in DhpA. In DhpA, Lys123 forms a hydrogen bond with the amide nitrogen atom of the nicotinamide ring and the Lys123 forms hydrogen bonds with two sulfonate oxygens of *R*- and *S*-DHPS. Residue Ser174 interacts with a sulfonate oxygens of *R*- and *S*-DHPS. Mutations of Lys123 or Ser174 to Gly significantly reduced DhpA activity towards both *R*- and *S*-DHPS (Fig. 2G and H), indicating their crucial role in negatively charged sulfonate group recognition, which effectively anchoring the sulfonyl group and stabilizing the substrate-enzyme complexes. The C3-OH of *R*- or *S*-DHPS is positioned in close proximity to Lys171, Asn175, and the NAD^+ nicotinamide, facilitating efficient proton and electron transfer. All these amino acid residues results in the formation of a more compact active site pocket that effectively encapsulates the *R*- or *S*-DHPS, and ultimately facilitate the appropriate juxtaposition of functional groups within the active site pocket.

3.3. The pathway for DHPS catabolism in bacteria

Sequence comparisons revealed DhpA homologs in sulfate-reducing bacteria inhabiting diverse environments, including sewage, sediments, and deep-sea cold seeps (Supplementary Table S4). Phylogenetic analysis placed these bacteria within the *Desulfovibrionaceae* family, suggesting the potential conservation of the DHPS metabolic pathway among this microbial group (Fig. 3A). These homologs displayed high amino acid identity (60–80 %) with DhpA from *Desulfovibrio* sp. DF1. Sequence alignments and structural comparisons demonstrated the conservation of key residues involved in DHPS binding and catalysis (Lys171, Lys123, Ser174, and Asn175) among these homologs. Furthermore, all homologs shared the Rossmann-fold domain for dinucleotide binding (Fig. 3B), exhibiting RMSD values <2.0 Å compared to the DhpA structure from *Desulfovibrio* sp. DF1 (Fig. 3C). These findings strongly suggested a conserved binding and catalytic mechanism among these bacterial homologs.

Analyses revealed that the *dhpA* gene is co-localized within a single operon with several other genes, including *slaB* (encoding dehydrogenase for SLA degradation), a gene encoding nickel-dependent racemase (NdlR), *suyAB* (encoding sulfolactate (SL) lyase), genes encoding components of ABC transporter system or a triple ATP-independent periplasmic (TRAP) transporter system, and a genes encoding a regulator, in a sulfate-reducing bacterium (Fig. 4A, Supplementary Table S5). Within this cluster, *Ndlr* is adjacent to *suyAB* in *Desulfovibrio* sp. DF1, DHPS undergoes sequential oxidation to SL via SLA, catalyzed by two NAD^+-dependent dehydrogenases, DhpA and SlaB. Previous studies have demonstrated that *R*-SL serve as the substrate for SuyAB in *Methanococcus jannaschii* and *Chromohalobacter salexigens* [44]. Based on these observations, we hypothesize that NdlR functions as a racemase, catalyzing the conversion of *S*-SL to *R*-SL (Fig. 4B). This proposed racemization step would enable the metabolism of both DHPS enantiomers within a single organism, representing a unique metabolic strategy compared to previously described pathways.

4. Discussion

Microorganisms from diverse terrestrial and marine environments have evolved a variety of metabolic pathways for DHPS degradation [18,21,24,25]. Sulfate-reducing microorganisms in anaerobic environments, such as ocean sediments and the digestive tracts of marine and terrestrial animals, act as "terminal oxidizers" of fermentation products [45]. In these environments, DHPS degradation leads to the conversion of sulfonated sulfur into H_2S. DHPS metabolism also has implications for human health, as humans produce DHPS through the consumption of SQ-rich vegetables [23]. Unlike the strict enantioselectivity observed in enzymes from aerobic organisms, this study demonstrates that DhpA from anaerobic sulfate-reducing bacteria can efficiently cleave both *R*- and *S*-DHPS. Lys171 in DhpA acts as a catalytic residue, directly oxidizing the primary hydroxyls of both enantiomers without the need for substrate racemization. The stereoselectivity of an enzyme is significantly influenced by the steric hindrance within its binding pocket [46]. Specifically, both *R*- or *S*-DHPS are tightly bounded within the active site, interacting closely with residues such as Lys171, Asn175, Ser174, and Lys123. This active site is relatively spacious pocket and lacks significant steric hindrance [43], allowing for the efficient binding of both substrate enantiomers. Furthermore, the small size and inherent flexibility of the DHPS molecule, combined with its directional properties, likely facilitate the accommodation of both enantiomers within the binding site. The high conservation of these four residues (Lys171, Asn175, Ser174, and Lys123) across DhpA homologs underscores their critical role in enzyme function, as demonstrated by mutagenesis studies.

Enzymes involved in DHPS degradation exhibit significant variability in their catalytic properties (Supplementary Table S6). Notably, DhpA demonstrates a substantial increase in catalytic efficiency for both *R*- and *S*-DHPS. Specifically, the k_{cat}/K_M for *R*-DHPS is enhanced 20- to 500-fold, while the efficiency for *S*-DHPS is even more remarkable, ranging from 10- to 2000-fold. This high catalytic efficiency suggests that DhpA enables microorganisms to rapidly degrade substrates in competitive anaerobic environments, thereby facilitating efficient energy and nutrient acquisition. Given that DhpA homologs have been identified in other anaerobic sulfate-reducing bacteria, we hypothesize that other DHPS-degrading enzymes within these environments, such as DHPS-sulfolyase HpsG and DHPS-dehydratase HpfG, may also possess the capacity to simultaneously degrade both chiral forms of DHPS, although the activity of these enzymes on *R*-DHPS remains unverified [23].

The *dhpA*-containing gene cluster for DHPS degradation has been identified in diverse sulfate-reducing bacteria across various environments (Fig. 3C). These clusters frequently contain genes encoding ABC or TRAP transport systems, likely facilitating the uptake of DHPS from the surrounding environment. Notably, many transporters for organic substrates exhibit broad substrate specificity [47–49]. For instance, studies on ABC transporters involved in SQ degradation have shown that the periplasmic binding protein, SmoF, can recognize not only SQ but also sulfoquinovosyl glycerol and short-chain glycolipid sulfoquinovosyl diacylglyceride analogs. These transporters achieve substrate recognition primarily through conserved interactions with the SQ headgroup [50]. Given the structural similarities between *R*- and *S*-DHPS, we hypothesize that these transporters may also be capable of importing both enantiomers of DHPS.

The widespread occurrence of DHPS metabolic gene clusters suggests that sediments may serve as significant reservoirs for DHPS and are

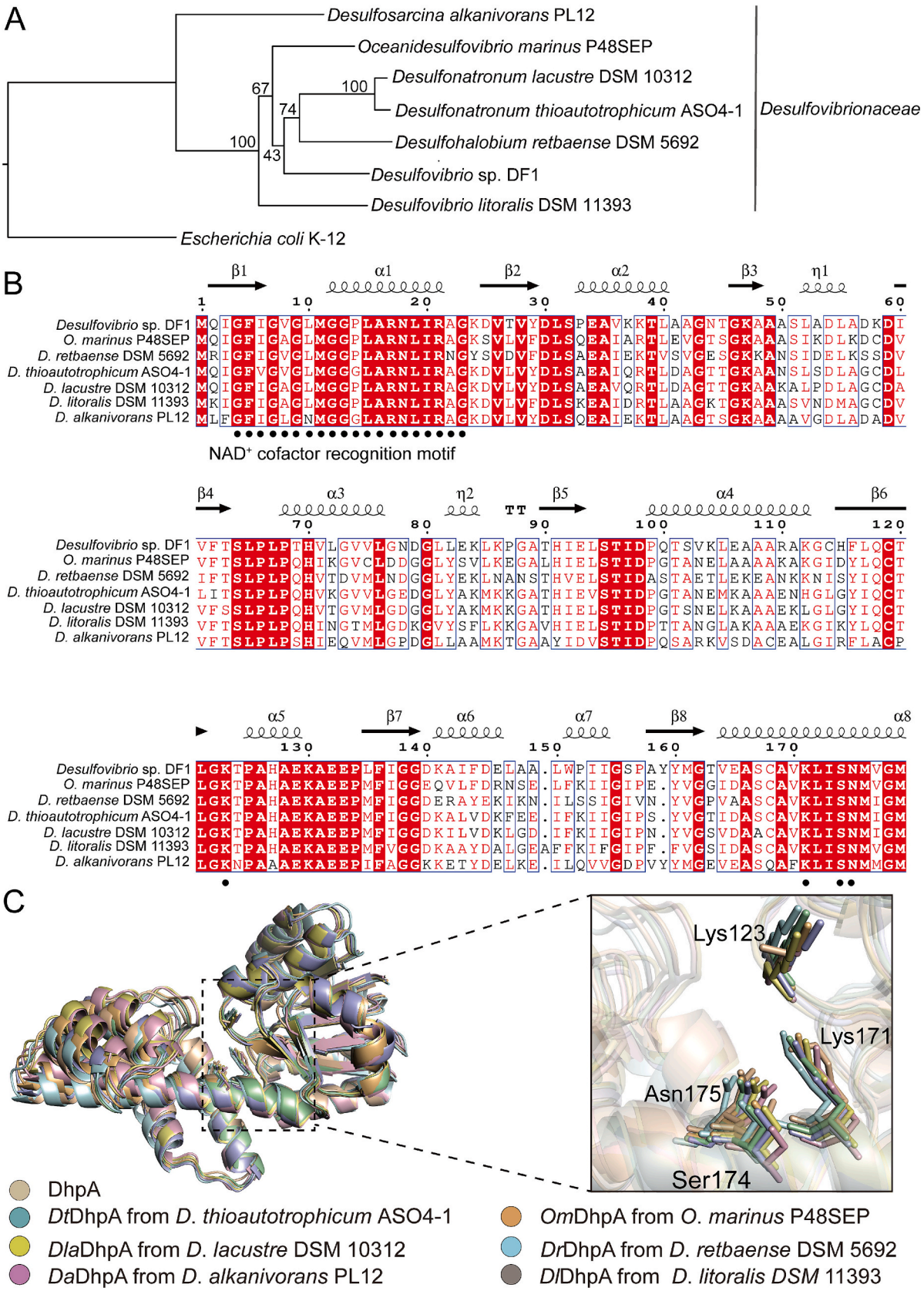


Fig. 3. Bioinformatic analysis of bacteria and DhpA homologs (A) Phylogeny of sulfate-reducing bacteria containing DhpA homologs. (B) Sequence alignment of selected regions of DhpA from *Desulfovibrio* sp. DF1 and its homologs. Numbers in parentheses refer to the amino acid numbers in the DhpA sequence. The dinucleotide-binding motif and residues involved in binding and catalysis are marked with black dots. (C) Crystal structure of DhpA and Alphafold2-predicted structures of *Om*DhpA, *Dr*DhpA, *Dt*DhpA, *Dla*DhpA, *Dl*DhpA and *Da*DhpA. The rod structures within the protein structure represent the residues conserved with Lys123, Lys171, Ser174 and Asn175 of DhpA.

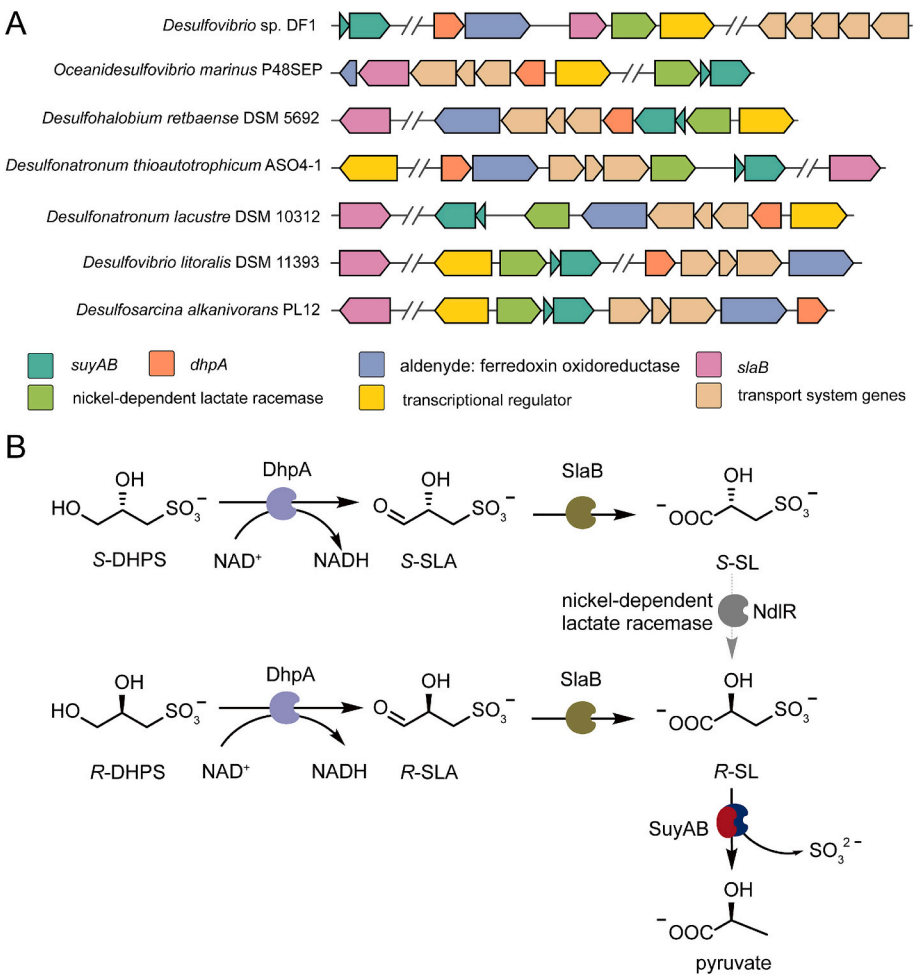


Fig. 4. Proposed degradation pathway of DHPS in *Desulfovibrio* sp. DF1. (A) Gene cluster encoding proteins involved in DHPS metabolism. Gene site tags and annotations are provided in Supplementary Table S5. Different colors represent gene functions. (B) The figure illustrates the sequential oxidation of DHPS to SLA by DhpA, followed by the oxidation of SLA to SL by SlaB. Finally, SL is cleaved by SuyAB to produce pyruvate and sulfite. The enzyme NdlR is likely involved in the racemization of *S*-SL to *R*-SL, enabling the degradation of both *R*-DHPS and *S*-DHPS.

active sites for its microbial cycling. While empirical evidence is still needed to fully support this hypothesis, the presence of *dhpA* in deep-sea cold seep bacteria implies a substantial role for DHPS in the broader marine sulfur cycle (Fig. 3C). The ability of DhpA to catalyze the degradation of both *R*- and *S*-DHPS endows bacteria with enhanced metabolic versatility, facilitating efficient substrate acquisition and utilization within their respective environments.

5. Conclusion

This study characterizes DhpA, a DHPS-degrading enzyme from sulfate-reducing bacteria, uniquely capable of metabolizing both *R*- and *S*-DHPS enantiomers. Structural and biochemical analyses, including identification of key catalytic residues (Lys123, Ser174, Asn175, and Lys171), reveal a conserved binding pocket accommodating both enantiomers. These findings uncover a chiral DHPS degradation pathway in bacteria, expanding our understanding of microbial strategies for utilizing chiral molecules in anaerobic environments.

CRediT authorship contribution statement

Xiaoyi Ma: Writing – original draft, Methodology, Investigation, Formal analysis, Data curation. **Huanyu Wang:** Writing – original draft, Methodology. **Le Liu:** Formal analysis, Data curation. **Hongyue Dang:** Formal analysis, Data curation. **Kai Tang:** Writing – original draft, Methodology, Investigation, Formal analysis, Data curation.

Declaration of competing interest

The authors declare that they have no known competing financial interests or personal relationships that could have appeared to influence the work reported in this paper.

Acknowledgments

This study was supported by the National Natural Science Foundation of China project (42188102, 92251306, 42141003, 42076160). This paper contributes to the science plan of the Global Ocean Negative Carbon Emissions (Global ONCE) Program.

Appendix A. Supplementary data

Supplementary data to this article can be found online at https://doi.org/10.1016/j.ijbiomac.2025.141806.

Data availability

The protein structure of DhpA was deposited in Protein Data Bank database (https://www.rcsb.org/) under access code 9K2J. doi: https://doi.org/10.2210/pdb9K2J/pdb.

References

[1] G.T.M. Bitchagno, V.A. Nchiozem-Ngnitedem, D. Melchert, S.A. Fobofou, Demystifying racemic natural products in the homochiral world, Nat. Rev. Chem. 6 (11) (2022) 806–822, https://doi.org/10.1038/s41570-022-00431-4.

[2] B. Sharma, Nature of chiral drugs and their occurrence in environment, J. Xenobiot. 4 (1) (2014) 2272, https://doi.org/10.4081/xeno.2014.2272.

[3] T.L.V. Ulbricht, Chirality and the origin of life, Nature 258 (5534) (1975) 383–384, https://doi.org/10.1038/258383a0.

[4] R. Wang, Z. Zhang, J. Sun, N. Jiao, Differences in bioavailability of canonical and non-canonical *D*-amino acids for marine microbes, Sci. Total Environ. 733 (2020) 139216, https://doi.org/10.1016/j.scitotenv.2020.139216.

[5] B.T. Williams, J.D. Todd, A day in the life of marine sulfonates, Nat. Microbiol. 4 (2019) 1610–1611, https://doi.org/10.1038/s41564-019-0576-5.

[6] C. Liu, K. Ma, L. Jiang, X. Liu, Y. Tong, S. Yang, X. Jin, Y. Wei, Y. Zhang, Bacterial cysteate dissimilatory pathway involves a racemase and *D*-cysteate sulfo-lyase, J. Biol. Chem. 300 (6) (2024) 107371, https://doi.org/10.1016/j.jbc.2024.107371.

[7] Ü. Kolukisaoglu, *D*-amino acids in plants: sources, metabolism, and functions, Int. J. Mol. Sci. 21 (15) (2020) 5421, https://doi.org/10.3390/ijms21155421.

[8] A. Alena, A. Laura, C. Felipe, New insights into the mechanisms and biological roles of D-amino acids in complex eco-systems, Front. Microbiol. 9 (2018) 683, https://doi.org/10.3389/fmicb.2018.00683.

[9] K. Das, H. Balaram, K. Sanyal, Amino acid chirality: stereospecific conversion and physiological implications, ACS Omega 9 (5) (2024) 5084–5099, https://doi.org/10.1021/acsomega.3c08305.

[10] D.D. Clark, J.M. Boyd, S.A. Ensign, The stereoselectivity and catalytic properties of Xanthobacter autotrophicus 2-[(R)-2-Hydroxypropylthio]ethanesulfonate dehydrogenase are controlled by interactions between C-terminal arginine residues and the sulfonate of coenzyme M, Biochemistry 43 (21) (2004) 6763–6771, https://doi.org/10.1021/bi049783h.

[11] L.A. Nguyen, H. He, C. Pham-Huy, Chiral drugs: an overview, Int. J. Biomed. Sci. 2 (2) (2006) 85–100.

[12] G. Zhang, H.J. Sun, Racemization in reverse: evidence that *D*-amino acid toxicity on Earth is controlled by bacteria with racemases, PLoS One 9 (3) (2014) e92101, https://doi.org/10.1371/journal.pone.0092101.

[13] M.T. Reetz, A. Zonta, K. Schimossek, K.E. Jaeger, K. Liebeton, Creation of enantioselective biocatalysts for organic chemistry by in vitro evolution, Angew. Chem. Int. Edit. 36 (24) (1997) 2830–2832, https://doi.org/10.1002/anie.199728301.

[14] K. Liebeton, A. Zonta, K. Schimossek, M. Nardini, D. Lang, B.W. Dijkstra, Directed evolution of an enantioselective lipase, Chem. Biol. 7 (9) (2000) 709–718, https://doi.org/10.1016/S1074-5521(00)00015-6.

[15] D.A. Lang, M.L.M. Mannesse, G.H. De Haas, H.M. Verheij, B.W. Dijkstra, Structural basis of the chiral selectivity of *Pseudomonas cepacia* lipase, Eur. J. Biochem. 254 (2) (1998) 333–340, https://doi.org/10.1046/J.1432-1327.1998.2540333.X.

[16] A.R. Autry, J.W. Fitzgerald, Sulfonate S: a major form of forest soil organic sulfur, Biol. Fertil. Soils 10 (1) (1990) 50–56, https://doi.org/10.1007/BF00336124.

[17] B.P. Durham, A.K. Boysen, L.T. Carlson, R.D. Groussman, K.R. Heal, K.R. Cain, R. L. Morales, S.N. Coesel, R.M. Morris, A.E. Ingalls, E.V. Armbrust, Sulfonate-based networks between eukaryotic phytoplankton and heterotrophic bacteria in the surface ocean, Nat. Microbiol. 4 (10) (2019) 1706–1715, https://doi.org/10.1038/s41564-019-0507-5.

[18] K. Denger, M. Weiss, A.K. Felux, A. Schneider, C. Mayer, D. Spiteller, T. Huhn, A. M. Cook, D. Schleheck, Sulphoglycolysis in *Escherichia coli* K-12 closes a gap in the biogeochemical sulphur cycle, Nature 507 (7490) (2014) 114–117, https://doi.org/10.1038/nature12947.

[19] P. Abayakoon, Y. Jin, J.P. Lingford, M. Petricevic, A. John, E. Ryan, J.W.Y. Mui, D. E.V. Pires, D.B. Ascher, G.J. Davies, E.D. Goddard-Borger, S.J. Williams, Structural and biochemical insights into the function and evolution of sulfoquinovosidases, ACS Cent. Sci. 4 (9) (2018) 1266–1273, https://doi.org/10.1021/acscentsci.8b00453.

[20] X. Chen, L. Liu, X. Gao, X. Dai, K. Tang, Metabolism of chiral sulfonate compound 2,3-dihydroxypropane-1-sulfonate (DHPS) by Roseobacter bacteria in marine environment, Environ. Int. 157 (13) (2021) 106829, https://doi.org/10.1016/j.envint.2021.106829.

[21] J. Mayer, T. Huhn, M. Habeck, K. Denger, K. Hollemeyer, A.M. Cook, 2,3-Dihydroxypropane-1-sulfonate degraded by *Cupriavidus pinatubonensis* JMP134: purification of dihydroxypropanesulfonate 3-dehydrogenase, Microbiology 156 (5) (2010) 1556–1564, https://doi.org/10.1099/mic.0.037580-0.

[22] A. Burrichter, K. Denger, P. Franchini, T. Huhn, N. Müller, D. Spiteller, Anaerobic degradation of the plant sugar sulfoquinovose concomitant with H_2S production: *Escherichia coli* K-12 and *Desulfovibrio* sp. strain DF1 as co-culture model, Front. Microbiol. 9 (2018) 02792, https://doi.org/10.3389/fmicb.2018.02792.

[23] J. Liu, Y. Wei, L. Lin, L. Teng, J. Yin, Q. Lu, J. Chen, Y. Zheng, Y. Li, R. Xu, W. Zhai, Y. Liu, Y. Liu, P. Cao, E. Ang, H. Zhao, Z. Yuchi, Y. Zhang, Two radical-dependent mechanisms for anaerobic degradation of the globally abundant organosulfur compound dihydroxypropanesulfonate, Proc. Natl. Acad. Sci. USA 117 (27) (2020) 15599–15608, https://doi.org/10.1073/pnas.2003434117.

[24] L. Liu, X. Gao, C. Dong, H. Wang, X. Chen, X. Ma, S. Liu, Q. Chen, D. Lin, N. Jiao, K. Tang, Enantioselective transformation of phytoplankton-derived dihydroxypropanesulfonate by marine bacteria, ISME J 18 (1) (2024) wrae084, https://doi.org/10.1093/ismejo/wrae084.

[25] L. Burchill, A. Kaur, A. Nastasovici, M. Lee, S.J. Williams, Structural and kinetic insights into the stereospecific oxidation of *R*-2,3-dihydroxypropanesulfonate by DHPS-3-dehydrogenase from *Cupriavidus pinatubonensis*, Chem. Sci. 15 (38) (2024) 15757–15768, https://doi.org/10.1039/d4sc05114a.

[26] Z. Otwinowski, W. Minor, Processing of X-ray diffraction data collected in oscillation mode, Methods Enzymol. 276 (1997) 307–326, https://doi.org/10.1016/S0076-6879(97)76066-X.

[27] S. Reitz, A. Alhapel, L.O. Essen, A.J. Pierik, Structural and kinetic properties of a *β*-Hydroxyacid dehydrogenase involved in nicotinate fermentation, J. Mol. Biol. 382 (3) (2008) 802–811, https://doi.org/10.1016/j.jmb.2008.07.050.

[28] P. Emsley, K. Cowtan, Coot: model-building tools for molecular graphics, Acta Crystallogr. D. 60 (Pt 12 Pt 1) (2004) 2126–2132, https://doi.org/10.1107/S0907444904019158.

[29] P.D. Adams, R.W. Grosse-Kunstleve, L.W. Hung, T.R. Ioerger, A.J. McCoy, N. W. Moriarty, R.J. Read, J.C. Sacchettini, N.K. Sauter, T.C. Terwilliger, PHENIX: building new software for automated crystallographic structure determination, Acta Crystallogr. D. 58 (Pt 11) (2002) 1948–1954, https://doi.org/10.1107/s0907444902016657.

[30] R.A. Laskowski, J.A. Rullmannn, M.W. MacArthur, R. Kaptein, J.M. Thornton, AQUA and PROCHECK-NMR: programs for checking the quality of protein structures solved by NMR, J. Biomol. NMR 8 (4) (1996) 477–486, https://doi.org/10.1007/BF00228148.

[31] M. Sharma, P. Abayakoon, J.P. Lingford, R. Epa, A. John, Y. Jin, E.D. Goddard-Borger, G.J. Davies, S.J. Williams, Dynamic structural changes accompany the production of dihydroxypropanesulfonate by sulfolactaldehyde reductase, ACS Catal. 10 (4) (2020) 2826–2836, https://doi.org/10.1021/acscatal.9b04427.

[32] K.J. Pampa, N.K. Lokanath, N. Kunishima, R.V. Rai, The first crystal structure of NAD-dependent 3-dehydro-2-deoxy-D-gluconate dehydrogenase from *Thermus thermophilus* HB8, Acta Crystallogr. D Biol. Crystallogr. 70 (Pt 4) (2014) 994–1004, https://doi.org/10.1107/S1399004713034925.

[33] C. Zhang, M. Shine, A.M. Pyle, Y. Zhang, US-align: universal structure alignments of proteins, nucleic acids, and macromolecular complexes, Nat. Methods 19 (9) (2022) 1109–1115, https://doi.org/10.1038/s41592-022-01585-1.

[34] G.M. Morris, R. Huey, W. Lindstrom, M.F. Sanner, R.K. Belew, D.S. Goodsell, AutoDock4 and AutoDockTools4: automated docking with selective receptor flexibility, J. Comput. Chem. 30 (16) (2009) 2785–2791, https://doi.org/10.1002/jcc.21256.

[35] J.C. Phillips, R. Braun, W. Wang, J. Gumbart, E. Tajkhorshid, E. Villa, C. Chipot, R. D. Skeel, L. Kalé, K. Schulten, Scalable molecular dynamics with NAMD, J. Comput. Chem. 26 (16) (2005) 1781–1802, https://doi.org/10.1002/jcc.20289.

[36] L.T. Nguyen, H.A. Schmidt, A. von Haeseler, B.Q. Minh, IQ-TREE: a fast and effective stochastic algorithm for estimating maximum-likelihood phylogenies, Mol. Biol. Evol. 32 (1) (2015) 268–274, https://doi.org/10.1093/molbev/msu300.

[37] J.D. Thompson, T.J. Gibson, D.G. Higgins, Multiple sequence alignment using ClustalW and ClustalX, Curr. Protoc. Bioinformatics Chapter 2 (Unit 2.3) (2002), https://doi.org/10.1002/0471250953.bi0203s00.

[38] J. Jumper, R. Evans, A. Pritzel, T. Green, M. Figurnov, O. Ronneberger, K. Tunyasuvunakool, R. Bates, A. Žídek, A. Potapenko, A. Bridgland, C. Meyer, S. A. Kohl, A.J. Ballard, A. Cowie, B. Romera-Paredes, S. Nikolov, R. Jain, J. Adler, T. Back, S. Petersen, D. Reiman, E. Clancy, M. Zielinski, D. Hassabis, Highly accurate protein structure prediction with AlphaFold, Nature 596 (7873) (2021) 583–589, https://doi.org/10.1038/s41586-021-03819-2.

[39] J. Rozewicki, S. Li, K.M. Amada, D.M. Standley, K. Katoh, MAFFT-DASH: integrated protein sequence and structural alignment, Nucleic Acids Res. 47 (W1) (2019) W5–W10, https://doi.org/10.1093/nar/gkz342.

[40] X. Robert, P. Gouet, Deciphering key features in protein structures with the new ENDscript server, Nucleic Acids Res. 42 (W1) (2014) W320–W324, https://doi.org/10.1093/nar/gku316.

[41] M.V. Kempen, S.S. Kim, C. Tumescheit, M. Mirdita, J. Lee, C.L.M. Gilchrist, J. Söding, M. Steinegger, Fast and accurate protein structure search with Foldseek, Nat. Biotechnol. 42 (2024) 243–246, https://doi.org/10.1038/s41587-023-01773-0.

[42] A. Tchigvintsev, A. Singer, G. Brown, R. Flick, E. Evdokimova, K. Tan, C. F. Gonzalez, A. Savchenko, A.F. Yakuni, Biochemical and structural studies of uncharacterized protein PA0743 from *Pseudomonas aeruginosa* revealed NAD^+-dependent L-serine dehydrogenase*, J. Biol. Chem. 287 (3) (2012) 1874–1883, https://doi.org/10.1074/jbc.M111.294561.

[43] S.C. Park, P.H. Kim, G.S. Lee, S.G. Kang, H.J. Ko, S. Yoon, Structural and biochemical characterization of the Bacillus cereus 3-hydroxyisobutyrate dehydrogenase, Biochem. Biophys. Res. Commun. 474 (3) (2016) 522–527, https://doi.org/10.1016/j.bbrc.2016.04.126.

[44] K. Denger, A.M. Cook, Racemase activity effected by two dehydrogenases in sulfolactate degradation by *Chromohalobacter salexigens*: purification of (*S*)-sulfolactate dehydrogenase, Microbiology 156 (3) (2010) 967–974, https://doi.org/10.1099/mic.0.034736-0.

[45] C. Pelikan, K. Wasmund, C. Glombitza, B. Hausmann, C.W. Herbold, M. Flieder, A. Loy, Anaerobic bacterial degradation of protein and lipid macromolecules in subarctic marine sediment, ISME J. 15 (3) (2021) 833–847, https://doi.org/10.1038/s41396-020-00817-6.

[46] K. Wu, Z. Yang, X. Meng, R. Chen, J. Huang, L. Shao, Engineering an alcohol dehydrogenase with enhanced activity and stereoselectivity toward diarylketones: reduction of steric hindrance and change of the stereocontrol element, Cat. Sci. Technol. 10 (6) (2020) 1650–1660, https://doi.org/10.1039/C9CY02444A.

[47] L. Sun, A.R.J. Curson, J.D. Todd, A.W.B. Johnston, Diversity of DMSP transport in marine bacteria, revealed by genetic analyses, Biogeochemistry 110 (1–3) (2012) 121–130, https://doi.org/10.1007/s10533-011-9666-z.

[48] L. Teichmann, H. Kummel, B. Warmbold, E. Bremer, OpuF, a new Bacillus compatible solute ABC transporter with a substrate-binding protein fused to the

trans membrane domain, Appl. Environ. Microbiol. 84 (20) (2018), https://doi.org/10.1128/AEM.01728-18 e01728-18.
[49] S.E. Noell, S.J. Giovannoni, SAR11 bacteria have a high affinity and multifunctional glycine betaine transporter, Environ. Microbiol. 21 (7) (2019) 2559–2575, https://doi.org/10.1111/1462-2920.14649.
[50] A.J.D. Snow, M. Sharma, J.P. Lingford, Y. Zhang, J.W.Y. Mui, R. Epa, E. D. Goddard-Borger, S.J. Williams, G.J. Davies, The sulfoquinovosyl glycerol binding protein SmoF binds and accommodates plant sulfolipids, Curr. Opin. Struct. Biol. 4 (2022) 51–58, https://doi.org/10.1016/j.crstbi.2022.03.001.